PONTIFICIA UNIVERSIDAD CATOLICA DE CHILE
ESCUELA DE INGENIERIA

# ENERGY DISSIPATION PARTITION WALLS

**JOSÉ TOMÁS RODRÍGUEZ VALDÉS**

Tesis para optar al grado de
Magíster en Ciencias de la Ingeniería

Profesor Supervisor:
JUAN CARLOS DE LA LLERA

Santiago de Chile, Noviembre 2011

PONTIFICIA UNIVERSIDAD CATOLICA DE CHILE
ESCUELA DE INGENIERIA

# ENERGY DISSIPATION PARTITION WALL

**JOSÉ TOMÁS RODRÍGUEZ VALDÉS**

Tesis presentada a la Comisión integrada por los profesores:

**JUAN CARLOS DE LA LLERA M.**

**JOSÉ LUIS ALMAZÁN C.**

**EDUARDO IZQUIERDO V.**

**CARLOS VIDELA C.**

Para completar las exigencias del grado de
Magíster en Ciencias de la Ingeniería

Santiago de Chile, Noviembre 2011

To Atilio and Manuel

## ACKNOWLEDGEMENTS

The author thanks the Chilean National Commission for Research in Science and Technology, CONICYT, for sponsoring this work through Grants Fondecyt N° 1110377, and Fondef N° D07I1006. The author also thanks ARMAS for their financial support on the investigation.

Special thanks to all the people involved who made this work possible: his supervisor Prof. Juan Carlos de la Llera, the people of DICTUC and SIRVE, his friends of the program and particularly the people of the Structural Engineering Laboratory.

Finally, the author wishes to express his deepest gratitude to his family for their constant and silent support.

## CONTENTS

## LIST OF TABLES

## LIST OF FIGURES

## RESUMEN

Entre los diferentes tipos de daño producidos en edificios debido al Terremoto de Chile de 2010 de $M_w$=8.8, se destaca el daño de elementos no estructurales y, particularmente, el de tabiquería. El daño de estos elementos causó la evacuación de una gran cantidad de edificios residenciales, provocando una angustia enorme en la población. Este hecho motivó el desarrollo de un modo de protección alternativo de bajo costo de la tabiquería típica compuesta por una estructura de acero cubierta por planchas de yeso cartón. Esta protección consiste en disipadores de energía metálicos en forma de U (UFP), que actúan como fusibles entre la tabiquería y la estructura. Este dispositivo, además de proteger la integridad del panel, aumenta del amortiguamiento del edificio, mejorando su comportamiento sísmico. El desarrollo de la nueva tabiquería disipadora se realizó a partir de ensayos experimentales de 7 tabiques convencionales y 3 modificados. También se realizó un extenso estudio numérico y experimental de los disipadores de acero liviano UFP. Para el último tabique disipador ensayado se obtuvo que la deformación de las planchas de yeso se redujo en un 78% con respecto a las del convencional, mientras que la energía disipada fue 5 veces mayor. Además de lo anterior, el comportamiento cíclico con "*pinching effect"* característico de planchas de yeso al degradarse fue prácticamente eliminado.



Palabra clave: Elemento no estructural, tabiquería, planchas de yeso cartón, disipación de energía, disipadores UFP, daño no estructural

## ABSTRACT

Among the various types of damage suffered by buildings, nonstructural one in partition walls was particularly prominent during the $M_w$=8.8, 2010, Chile earthquake. Such damage caused a great number of residential facilities to be evacuated, causing tremendous social distress and anxiety in the various communities. Motivated by this fact, this article discusses a low-cost alternative to protect the usual steel framing and gypsum sheathed partition walls, by using a metallic energy dissipation based on U-shape elements, which act as mechanical fuses in series with the panel. Besides protecting the integrity of the panel, the proposed elements add in a seamless way supplemental damping to the building, thus enhancing its seismic performance. The development process of the new dissipative partition wall was based on experimental testing of 7 conventional partition walls, and 3 different modified walls. Extensive numerical and experimental analyses of thin-plate UFP dampers were also performed. For the last proof-of-concept equipped partition wall, the deformations on the gypsum boards were 78% less than those of the conventional one, while the energy dissipated was 5 times larger. Moreover, the cyclic pinching effect, which is characteristic of conventional degrading partitions, was essentially eliminated.



Keyword: Nonstructural components, partition wall, gypsum boards, energy dissipation, UFP dampers, nonstructural damage

# 1. INTRODUCTION

Recent earthquakes [7] have reiterated the importance of the seismic performance of non-structural components in buildings leading to operational and safety issues, and economical loss. Substantial seismic damage of non-structural components occurred in mid- and high-rise buildings during the February 27, 2010, Chile earthquake [5]. Non-structural damage caused major disruption of normal activities and closure of an important number of facilities, including warehouses, hospitals, and the SCL airport. A significant portion of the economic loss can be attributed to failure of non-structural components and disruption of functionality [e.g., 5].

Among the most damaged non-structural components in buildings were partition walls (PW) [5]. Their typical cost per square meter ranges (in Chile) from 20 to 25 US$/m$^2$, which corresponds to about 5% of the non-structural cost of the building [27]. Partitions are not intended as lateral or vertical load-carrying elements, rather as interior architectural elements designed to divide spaces.

Light-gauge steel framing sheathed using gypsum boards is a common non-structural PW solution and several studies have investigated their seismic performance [11-23]. The main research focus has been on the evaluation of their cyclic performance under imposed inter-story deformations, and to establish the corresponding damage thresholds. The influence of connection details, different opening configurations, door inclusion, deformation histories, have all been investigated. Also, the interaction between partitions and other non-structural components [18,19], relationships for drift-repair costs [17], and the influence of PW in the response of the main structural system,

have also been studied from an analytical [11] and experimental perspective, the latter by testing a full-scale 4-story building model [18].

In order to protect integrity, well-constructed PW are usually disconnected from the primary structural system [18]. Such disconnection of the gypsum boards, the most expensive and fragile element of the wall, is attained by leaving gaps between the boards and the floor and ceiling, and by placing the vertical steel framing members or studs without any screw attachment to the top and bottom runners, which are fixed to the slab.As the building sways, this assembly produces horizontal and vertical sliding of the studs, which enables a mechanism-like behaviour of the PW, and eventually, less resistance to the imposed inter-story deformations. Although conceptually correct, this separation between the PW and the main structure is not always achieved in practice as the PW is sometimes fixed to the structure through windows or doorways, encounter other perpendicular PW, or are attached to other structural components. In such case, considerably damage may occur [17,19], and operational as well as safety aspects such as door jamming [16] and blocking of evacuation exits may occur. However, there are several other architectural aspects that are more cumbersome as the separation between PW and structure is enforced.

Therefore, an effective way to protect a PW from damage as the building sways is based on connecting a PW to the structure through an energy dissipation system and designing the assembly to work as a secondary structural component. Thus the PW is designed to undergo the required inter-story drift with no damage, by introducing in the so-called energy dissipating partition wall (EDPW) an ED-connector between the PW

and the structure. Besides protecting the integrity of the PW by limiting the forces transmitted to the PW, this connector has the advantage of introducing a controllable energy dissipation capacity inside the structure in a component that is usually regarded in the structure as exclusively architectural. The design proposed herein slightly modifies the conventional gypsum board PW. The ED-connectors are U-shaped flexural plates (UFP) [15], dissipators widely studied since the 1970's [e.g., 20,1]. The UFPs was chosen because of large deformation capacity, low cost, and simplicity of fabrication and maintenance.

A similar concept to the EDPW was developed on wooden shear-wall partitions with supplemental damping [26-25]. Shear walls are different from the non-structural ones since they are designed to carry lateral and vertical loads. However, both designs, that of the shear-wall and that of the EDPW, are both intended to protect the integrity of their components by dissipating the inter-story deformation energy. Several devices have been tested within shear walls, viscoelastic, viscous, frictional and hysteretic, with very promising results such as [4]. However, the sole installation procedure for these shear-walls, usually prefabricated panels, is more complex than including energy dissipation in PW that can be installed on site, maintaining the current installation procedure essentially unchanged.

Because of the complexity of the cyclic behaviour of the gypsum PW, the methodology used in this research to estimate the seismic performance was essentially experimental. It included an analysis of conventional PW under cyclic loading, the characterization of the critical screwed connection between the board and light-gauge

vertical stud elements, the shear behaviour of the UFP energy dissipation device, and the cyclic behaviour of the PW equipped with the UFP dissipators. In general terms, the goals of this research were to: (i) develop an architecturally seamless solution for the EDPW; (ii) generate a solution for the PW, which installation is similar to the conventional one; and (iii) maximize the energy dissipation capacity of the PW while protecting its integrity under cyclic loading.

## 2. PARTITION WALL DESCRIPTION

One of the most widely used partition element in buildings is the gypsum board partition wall (GB-PW). Its properties as a good thermal and acoustic insulator, as well as fire resistant element, in combination with its low cost and ease of installation, make the GB-PW a widely used component. However, its seismic performance depends significantly on the installation procedure, which varies according to the local construction practice [24]. A detailed description of the installation procedure is useful to understand the cyclic behaviour of the PW.

The PW investigated in this study consists on an inner light-gauge galvanized steel framing composed by C-shape vertical studs spaced every 40 cm, thickness of 0.85 mm, and sheathed at both faces by gypsum boards of thickness of 15 mm (Figure 2-1). According to the fire-resistant Chilean regulation, two main PW types are established according to their fire resistance requirements [13]: a) main separators—used to separate offices or departments (120 minutes of fire before reaching T=180 °C), and b) secondary separators—used to separate interior spaces of the same property (60 minutes of fire before reaching T°=180ºC) [21]. The PW type used in this investigation is the main separator. The height of the PW depends on the building inter-story height, but usually in office spaces is about 3 m; PW length varies greatly according to floor dimensions and plan layout. For instance, considering only the main partitions, a building plan of 1550 $m^2$ with 4 offices, PW length may require typically from 60 to 120 linear meters.

The PW installation does not required very skilled labour, but it follows a rigorous procedure since it is done to allow the PW to slide as a mechanism relative to

the floor slabs. Often, several factors impair this free sliding and movements of the panel, and hence, PW undergo permanent damage. For instance, by attaching the PW to the structure of the building, sliding is impeded around openings such as doorways and windows, or intersections with other PW or structural elements. These cases are usual in office buildings and the main cause of the most important damage underwent by the wall due to applied deformations in the longitudinal direction [17,19].

The installation procedure described next is based on current Chilean practice and suggested by GB manufacturer manuals. The installation is done in two sequential stages: the steel framing and sheathing (Figure 2-1(b)).

Initially, top and bottom runners are attached to the slabs by power-driven nails (Figure 2-1(c)) spaced at 40 cm, and starting and 5 cm from the runner edges (Figure 2-1(e)).Runners are ASTM630 gr.40 C-shaped channels of dimensions 62x25x0.85 mm; sometimes 0.5 mm steel shapes are used. Then, studs are pressure mounted on the runners and spaced at 40 cm; studs are U-shaped ASTM630 steel shapes 60x38x0.85 mm with flange return lips of 8 mm. A 5 mm gap is left between the end of the stud and the web of the runner to allow for vertical motion. Studs are not screwed to the runners, hence horizontal and vertical sliding between these elements is permitted (Figure 2-1(c)).

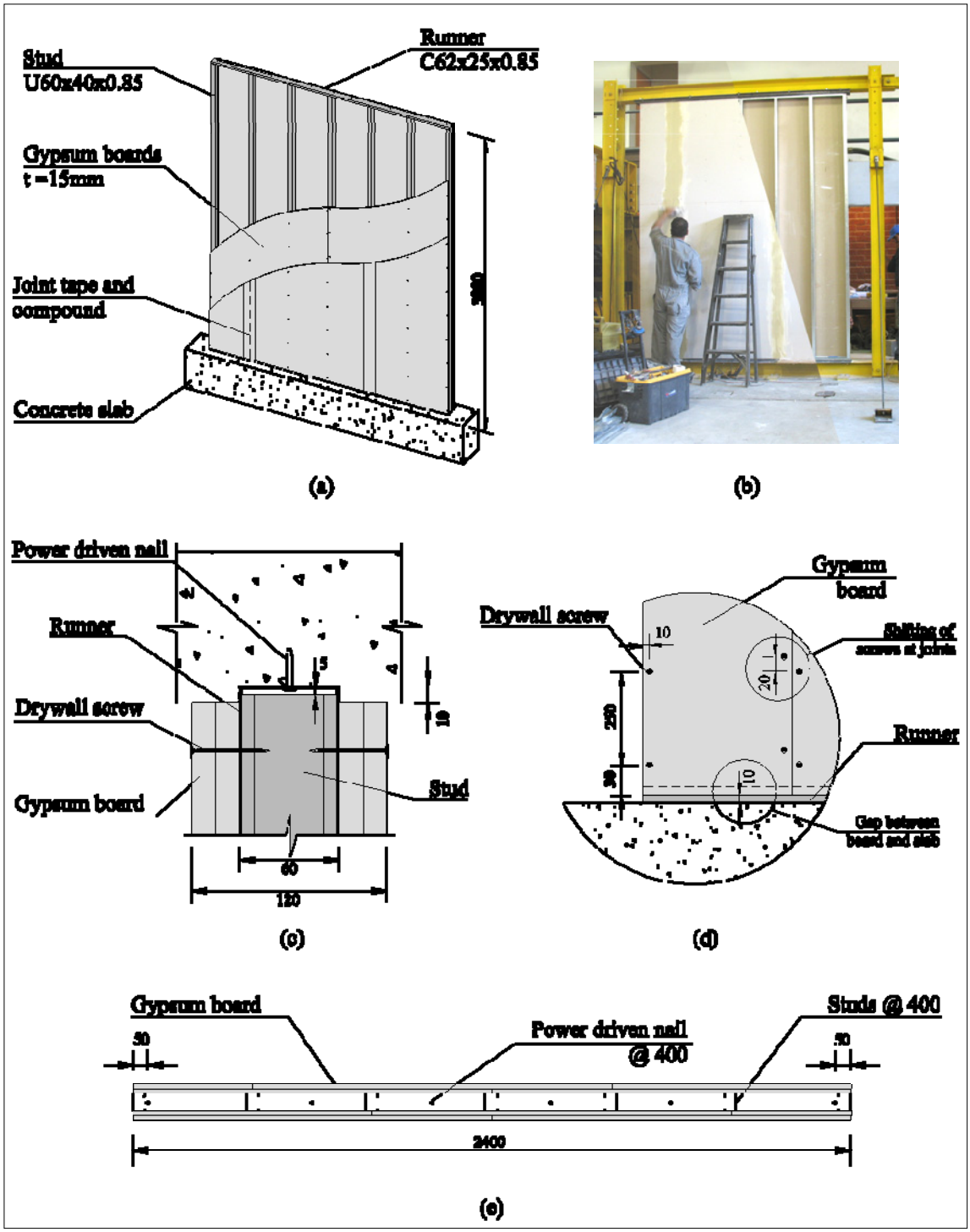


Figure 2-1: Conventional partition wall description: (a) general scheme, (b) photo of PW showing the inner framing, (c) section of top connection to slab, (d) corner detail of PW, and (b) plan section.

Sheathing consists of 2 gypsum boards of 12.5 or 15 mm in thickness on each face. The boards are attached only to the studs by 1½'' self-drilling drywall screws. A 1 cm gap is left between the top and bottom edges of the board and the concrete slab. Vertical board joints for the inside and outside boards are shifted half board to avoid the overlap of joints (Figure 2-1(a)). The screws are spaced vertically at 25 cm, at 1 cm of the board edges and 3 cm from the top and bottom edges. At the joints, the screws of one board are displaced on 2 cm relative to those of the other board. Distribution of screws is presented in Figure 2-1(d). After installed, joints are covered by gluing fibreglass tapes previous to finishing the PW with joint compound (Figure 2-1(a)).

## 3. STRUCTURAL BEHAVIOR OF CONVENTIONAL PW

Before proceeding with the design of a solution for an EDPW using a modification of a conventional PW, the lateral behaviour of the conventional wall attached to the concrete slabs must be analyzed. Shown in Figure 3-1 is a simplified model for better understanding of the different components of the lateral resistant system of the PW when subjected to a lateral displacement. More elaborated structural models have been proposed for light-gauge steel shear walls [e.g., 12,9].

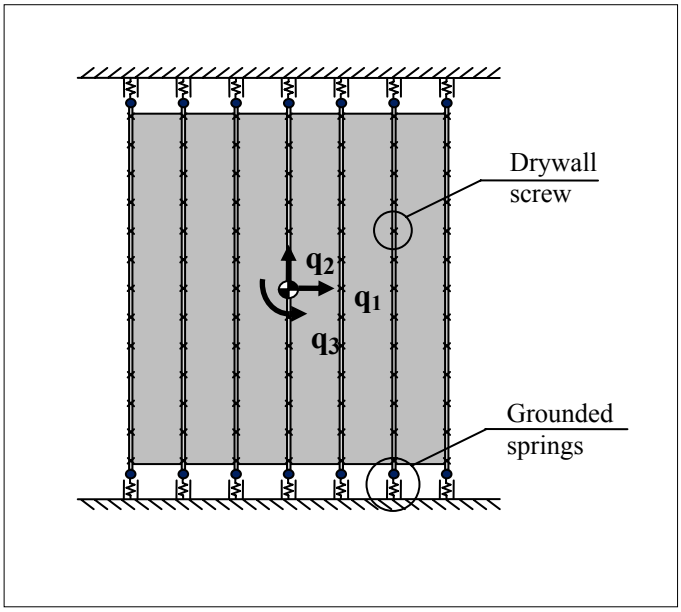


Figure 3-1: Simplified structural model of a partition wall.

The inner framing in the model is composed of two elements: a) the vertical flexural elements, the studs; and b) the springs that represent the connection of the stud to the runner and the runner to the slab, on top and bottom of the panel. This inner

framing is fixed to the structure by placing screws from the studs to the runners, so no sliding of the studs is allowed. This is modelled as a pinned connection, which makes the steel framing of the PW a mechanism for lateral motion. The screwing of the runners is made to represent the case when the PW suffers damage when its fixed to the structure, which is the PW to be modified into a EDPW. The properties of the spring element depend on the flexibility of the runners as they are pulled by the studs, and hence, it depends on the type of anchoring used for the runners. The runners will tend to uplift as the gypsum sheathing will try to accommodate the lateral displacement of the panel through rotation.

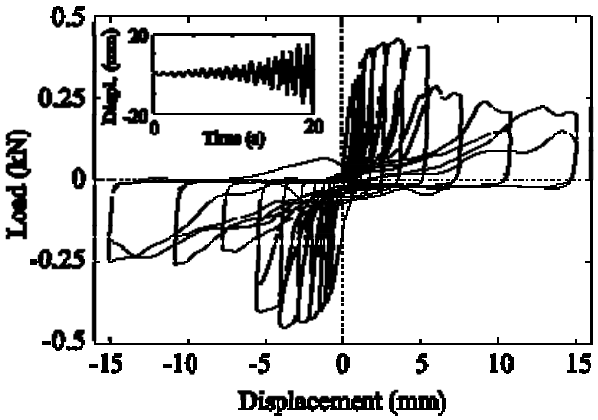


Figure 3-2: Hysteretic response of the drywall screw connection.

In this model, gypsum boards are considered as rigid vertical diaphragms. This implies that boards displace and rotate as a unity, their elasticity is negligible. Due to the gaps left between the boards and the top and bottom slabs, this motion will not introduce incompatibility with the lateral deformation. Therefore, the only stresses in the board

result from the incompatibility of motions between the vertical studs and gypsum boards.

The fastening of the boards to the studs through drywall screws may be represented by non-linear link elements; this type of connection was studied extensively earlier [8] and also herein. In our case, five probes were tested under cyclic displacements with increasing amplitude (Figure 3-2, inner box). Each probe was made of a 20 by 10 cm piece of a 15mm gypsum board attached to an ASTM A792 C60x40x0.5 mm steel stud connected through a drywall screw #6. These tests clearly showed that as the board moved, the screw pivoted at the perforation of the stud flange and damaged the perforation at the inner face of the board. As a result, the hysteresis loops obtained were dominated by pinching and stiffness degradation of the tested assembly (Figure 3-2). Important load decrease was observed for deformations over 5 mm.

Conceptually, the behaviour of the PW is conditioned by the motion of the board and this movement interacts with the three flexible elements described: a) the vertical stud elements, b) the connection of the studs and runners represented by the grounding springs, and c) the drywall and stud screwed connections. For the better understanding of the PW cyclic behaviour and interaction with each of its components, experimental measurement of the load-displacement constitutive behaviour was done.

Consequently, lateral testing of the conventional PW were designed and performed to obtain the cyclic performance of a conventional PW. Dynamic tests were performed on full-scale specimens. The loading frame was specially devised to

accurately replicate site conditions, and consisted of a pin-connected steel frame driven by a 25 ton MTS 244.31 dynamic actuator. The test setup is shown schematically in Figure 3-3 and allows panels of maximum dimension 321 cm high by 272 cm long. The testing frame has top and bottom beams W6 (6''x6''), and columns formed by C150x50x4 beams. The bottom beam was anchored to a foundation by expansion bolts and the top beam was connected through a mechanism to the 25 ton actuator. Omega steel shapes reinforced with stiffeners were bolted to the beams. The PW specimens were built in the testing frame and were anchored by the screwing of the runners to the omega shapes (Figure 3-3(b)).

A total of seven PW were tested as those presented earlier in Figure 2-1. A detail description of specimens is shown in Table 3-1. The construction procedure for the PW is identical to the one at the construction site with the exceptions that the studs were screwed to runners and runners were attached to the testing frame instead of the slabs. Three different types of full-scale PW were used, all 3 m in height and 2.4 m in length. The first group consists of walls with 0.5mm thickness for the steel framing, denoted as light partition walls (LPW). The second group had a 0.85mm steel framing, denoted as base partition wall (BPW). In the third group, PW also have 0.85mm framing, but the anchoring was reinforced, and it will be denoted as RPW.

The anchoring systems of specimens LPW and BPW were identical. Runners were anchored to the top and bottom testing frame elements by #7 7/16'' wafer head self-drilling screws at 5 cm from the edge of the runner and between studs spaced at 40 cm (Figure 2-1(e)). These screws mimic the power-driven nails used in concrete slabs,

so their head diameters match. For the RPW specimens, the anchoring was reinforced by using two screws instead of one, following the same spacing pattern as the other specimens. In all cases, studs were attached to runners by #8 ½'' self-drilling framer screws and a 5 mm gap was left between the end of the studs and the runners (Figure 3-3(b)).

The specimens were tested using a cyclic displacement history applied in two phases. The first phase was identical for all specimens and it was based on the protocol proposed by FEMA 461 [6]. The FEMA 461 describes protocols for testing buildings components mainly to establish their fragility functions for performance-based seismic design. However, these protocols may also be used to determine the hysteretic response for building components, including non-structural elements such as partition walls. The protocol used was the Quasi-Static Cyclic Testing (QSCT).

The first phase of the test consisted of 10 consecutive two-cycle steps of increasing amplitude—in geometric progression—with a scale factor of 1.4, and applied at a frequency of 0.1 Hz until reaching the target deformation. The target deformation corresponded to a maximum drift of 1%, and hence, for an inter-story height of 3m, the target deformation is 30 mm. This deformation is considered to be representative of the design drift expected in a building during a severe seismic event in Chile. After reaching the target deformation the test was paused for the observation of damage and removal of measurement instrumentation (LVDTs).

Two different protocols were used for the second phase of the test: six specimens were tested to large deformation and one to fatigue with constant displacement. The

protocol used for large deformations consisted of 5 consecutive two-cycle steps of increasing amplitude with a scale factor of 1.3 at 0.1 Hz, starting from 30 mm and reaching to a maximum amplitude of 110 mm. At this deformation amplitude the walls were expected to undergo severe damage, to which repairing costs may reach the initial cost of the PW [17]. The displacement history for the six specimens tested to large deformation is presented in Figure 3-4. For specimen BPW3 (Table 3-1) the second phase of the test corresponds to the application of 80 cycles at 30 mm amplitude and frequency 0.1Hz.

Measurements of the applied deformations and loads were obtained by the transducer and load cell of the actuator. The kinematics of the boards on one face was obtained by measuring displacements with four LVDTs as shown in Figure 3-3(a).Testing started 24 hours after the construction of the wall, to allow the joint compound to dry.

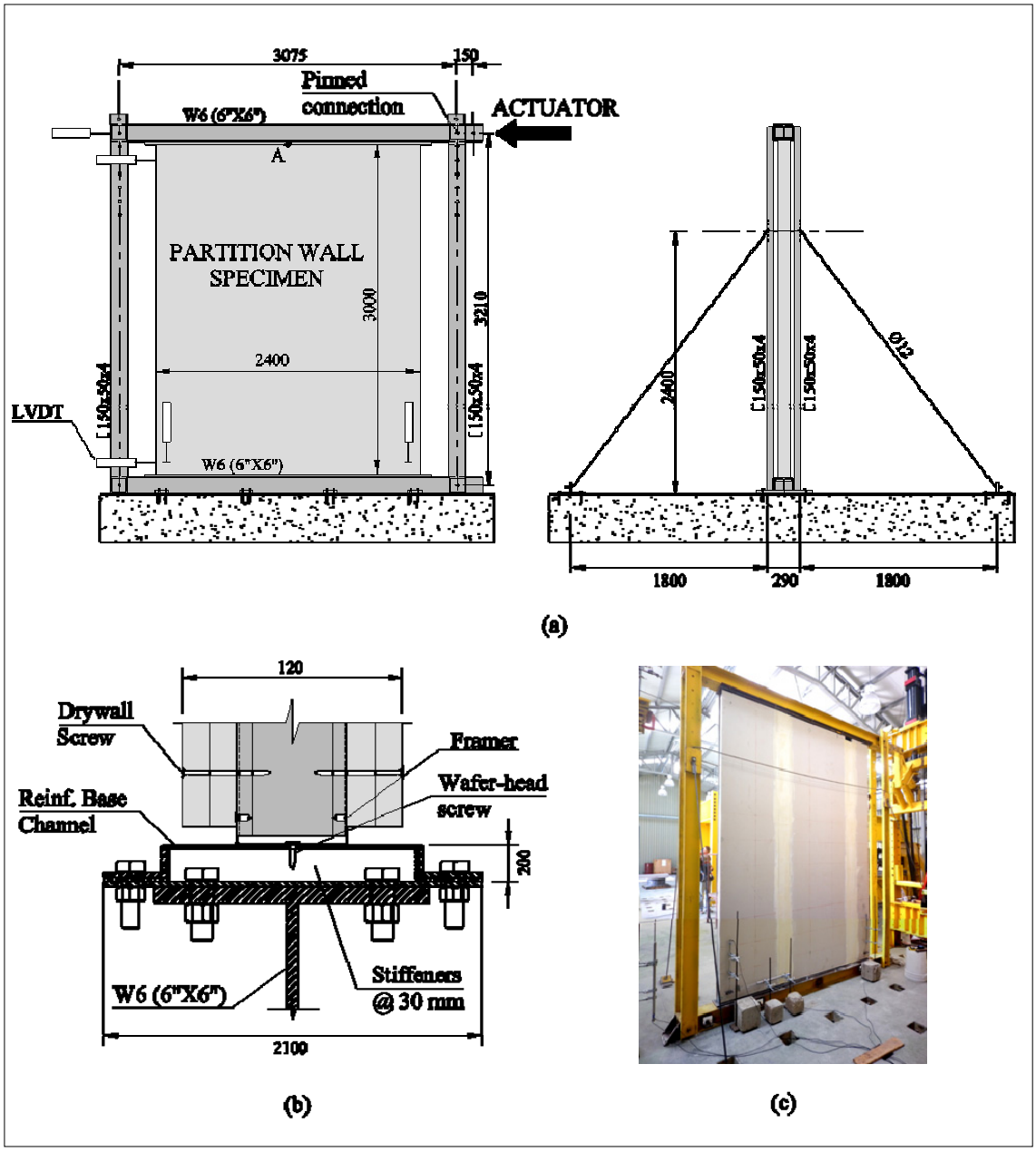


Figure 3-3: Set-up of tests of partition walls: (a) general elevation of testing frame and lateral elevation, (b) section of connection to bottom beam. (c) Installed specimen with instrumentation.

Table 3-1: Description of partition wall specimens

| Specimen | Steel Structure | | | |
|---|---|---|---|---|
| | Runner | Anchoring Screws | Stud | Runner-stud screws |
| LPW1-2 | **A792 C61x20x0.5** | 1 WH[(1)]-SD[(2)] #7 at 40 cm | **A792 U60x38x0.5** | 1 SD-F[(3)] #8 |
| BPW1-2-3 | **A630 C62x25x0.85** | 1 WH-SD #7 at 40 cm | **A630 U60x40x0.85** | 1 SD-F #8 |
| RPW1-2 | A630 C62x25x0.85 | **2 WH-SD #7 at 40 cm** | A630 U60x40x0.85 | 1 SD-F #8 |
| EDW1 | A630 C62x25x0.85 | 1 WH-SD #7 at 40 cm | A630 U60x40x0.85 | **2 SD-F #8** |
| EDW2 | same as EDW1 | **2 WH-SD #7 below studs** | same as EDW1 | same as EDW1 |
| EDW3 | same as EDW1 | **2 WH-SD #7 below studs + hold-downs** | same as EDW1 | same as EDW1 |

Note: All specimens were sheathed by 2 gypsum boards of 15 mm per side attached by SD drywall screws #6

[1] WH: wafer head
[2] SD: self-drilling;
[3] F: framer

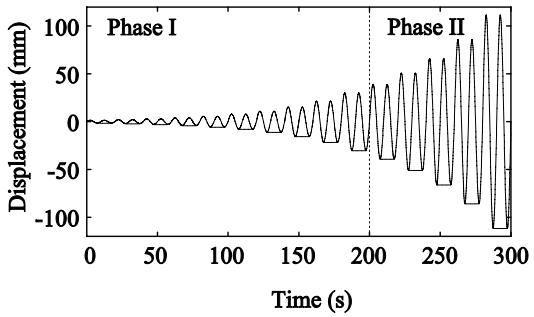


Figure 3-4: Displacement protocol for PW tests.

It is apparent from Figure 3-5 that the behaviour of all specimens of PW present similarities in terms of the shape of the force-deformation cycles, strength, stiffness and strength degradation. While the qualitative behaviour was dominated by the rigid body displacement and rotation of the boards, which behave like a single unit, the hysteresis loops were dominated by important pinching effects and a quick degradation in the PW stiffness.

In the first testing phase, rotation of the boards caused localized damage by pulling-off of the drywall screws at corners. Damage started at very small lateral displacements and it was present through the entire test with increasing severity and propagating from corners to the edges. Failure of the connection between the drywall and studs determines the hysteretic behaviour of the wall. Uplifting of the end studs by pulling up the runners was observed at displacements of about 20 mm; this led to an important increase in the rotation of the boards.

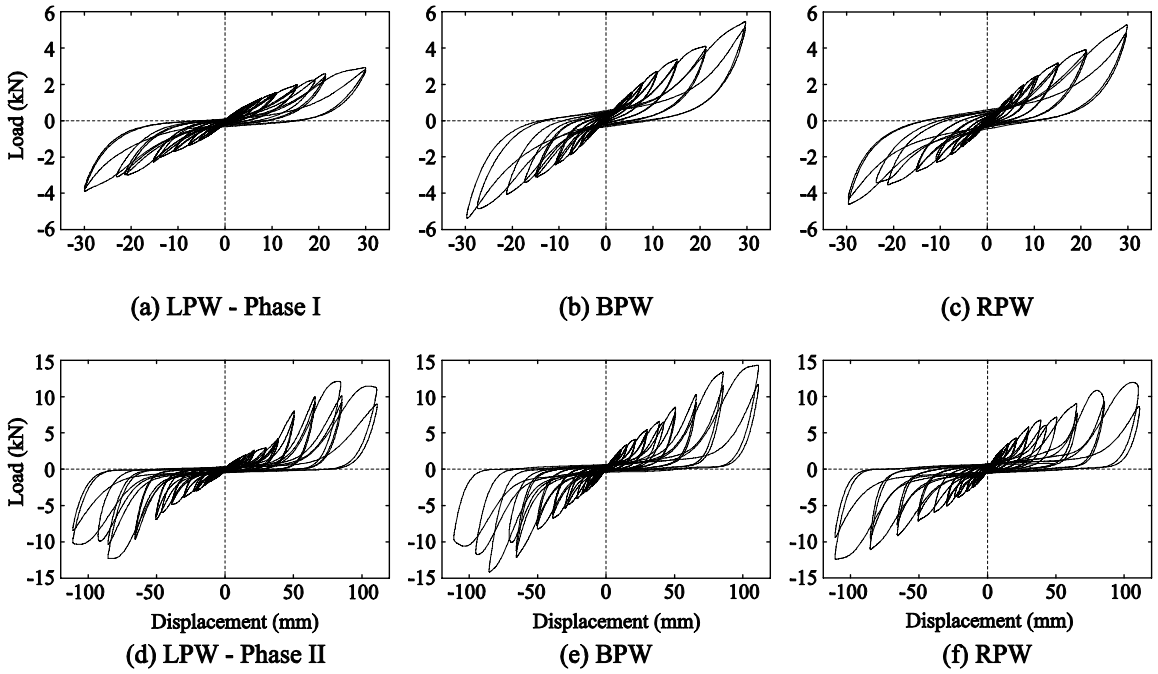


Figure 3-5: Hysteretic response of PWs: (a), (b) and (c) for Phase I of protocol, and (d), (e) and (f) for Phase II. Values per unit length of wall.

In the second phase, none of the six specimens tested to large deformation completely collapsed. At 110 mm, all specimens were still carrying load, despite of their severe damage. The most severely damaged wall was LPW because runners were considerably more flexible and uplift of the studs started earlier and were larger. Damage observed in specimens BPW and RPW was essentially the same.

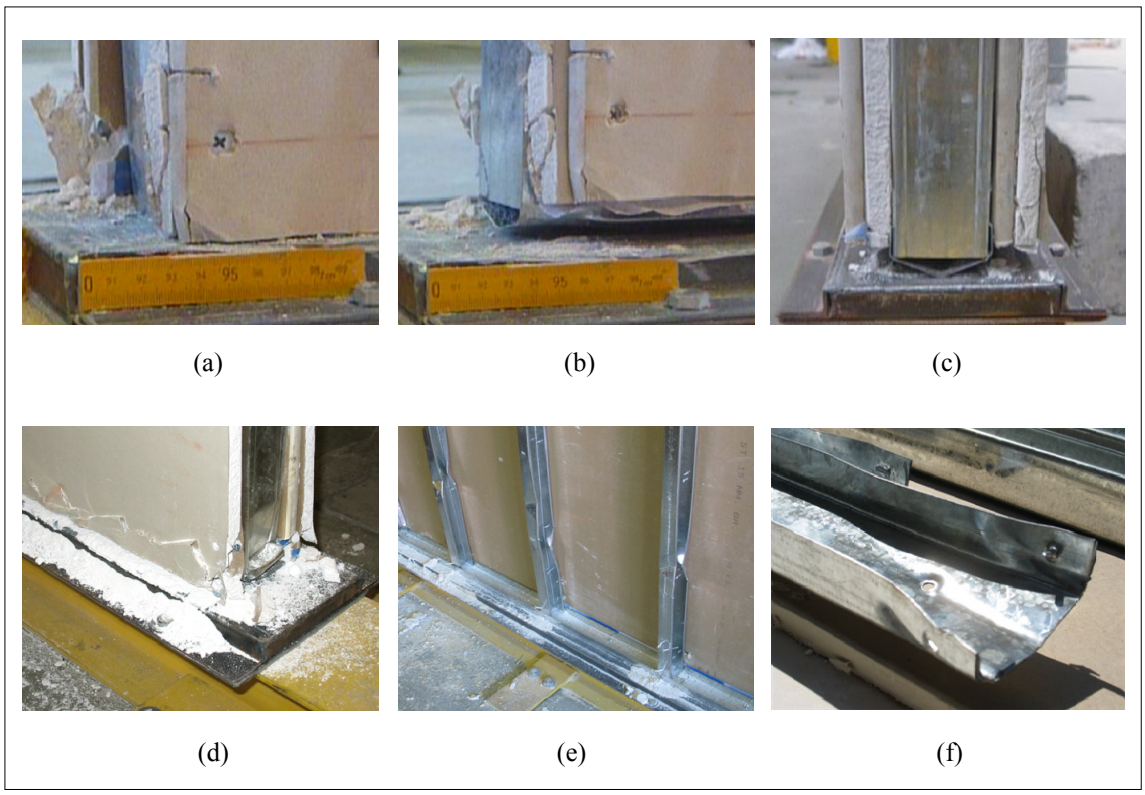


Figure 3-6: Photos of failure modes observed in PW tests: (a) pull-off of the screw, (b) pullo-off of the screw and uplifting of runner, (c) uplifting of runner, (d) crushing of boards, (e) local buckling of studs, and (f) deformation of the flanges of the runners. :

The failure modes observed on the tested specimens were: (i) pull-off of the screws at corners and vertical edges, leading in many cases to torn edges, also shown earlier in specimens of type LWP [23]; (ii) notorious uplifting of the outer studs and runners at the panel edges—for LPW caused tearing-off of the flanges of the runners, bearing failure of the screw connectors of studs, and failure of the connection of the runner and anchoring; (iii) local buckling of outer studs at the ends due to compression and deformation of the flanges of the runners; (iv) crushing of the board corners; (v) local buckling of all end studs at the bottom end (l=30cm); (vi) tearing-off of the joint

compound by the head of screws; and (vii) cracking of the joint compound. Observed cracks were not thicker than 1 mm and 20 cm long—a single important crack 4mm thick and 45 mm long was seen in specimen RPW1. Figure 3-6 shows pictures of various failure modes.

Table 3-2: Results of PW tests.

| Specimen | 15 mm deformation | | | 30 mm deformation | | | Max Load (kN) |
|---|---|---|---|---|---|---|---|
| | Load (kN) | Energy (J) | BDR[(1)] (%) | Load (kN) | Energy (J) | BDR (%) | |
| LPW1 | 1.4 | 12 | 97 | 2.9 | 46 | 95 | 11.9 |
| LPW2 | 2.1 | 16 | 92 | 3.4 | 62 | 90 | 12.3 |
| BPW1 | 2.8 | 22 | 88 | 5.2 | 89 | 85 | 12.7 |
| BPW2 | 3.0 | 26 | 86 | 4.9 | 88 | 86 | 14.3 |
| BPW3 | 2.6 | 24 | 86 | 4.2 | 82 | 84 | - |
| RPW1 | 2.6 | 27 | 87 | 5.0 | 97 | 86 | 12.4 |
| RPW2 | 3.1 | 30 | 88 | 4.6 | 92 | 89 | 11.3 |
| EDW1 | 1.8 | 19 | 82 | 3.7 | 68 | 82 | - |
| EDW2 | 2.4 | 24 | 71 | 4.1 | 104 | 72 | - |
| EDW3 | 2.2 | 59 | 28 | 2.4 | 187 | 18 | - |

Note: Values per unit length of wall

[1] BDR: Board/applied displacement ratio

To characterize the dynamic behaviour of PW, three response variables were used: a) load, b) dissipated energy, and c) the horizontal displacement of boards (BDR). Results for the first phase of the tests are presented in Table 3-2. For the load capacity

the force-displacement pushovers for each specimen are presented in Figure 3-7(a). The values used for these curves are calculated as the average between the maximum and the minimum load values for the first cycle for a given deformation. For displacements up to 30 mm, load capacity and stiffness of specimens of type BPW and RPW were similar, but for LPW they were considerably lower. On the other hand, the maximum load obtained for specimens of all types tested to large deformation were very much alike, as seen on Table 3-2. It can be deduced that thickness is relevant mainly on the stiffness of the PW, and for load capacity at large displacements the most important factor is the sheathing.

The energy dissipation of the PW is computed as the area enclosed by the first cycle of the force-displacement hysteretic loop for a given deformation. First phase results are shown in Figure 3-7(b). Energy dissipated by PW of type RPW was around a 10% larger than that of type BPW, difference observed from small displacements. Values for specimens LPW were considerably lower, and assuming that the energy dissipated comes principally from damage at the drywall screw connections, then these results show that deformation of the drywall screws is less due to the larger flexibility of the steel framing. In the same way, the strengthening of the anchoring on specimens of type RPW caused larger deformation of the screws due to stiffening of the framing. The integrity of the PW degrades considerably with repetitive cycles, as expected from the cyclic performance of the connection between gypsum board and steel stud observed from the tests described previously. To highlight this behaviour the ratio between the dissipated energy of the second cycle and the first cycle is presented in Figure 3-7(c).

The decrease for all specimens was around 20% to 30%, without showing any clear tendencies regarding the different types of PW tested.

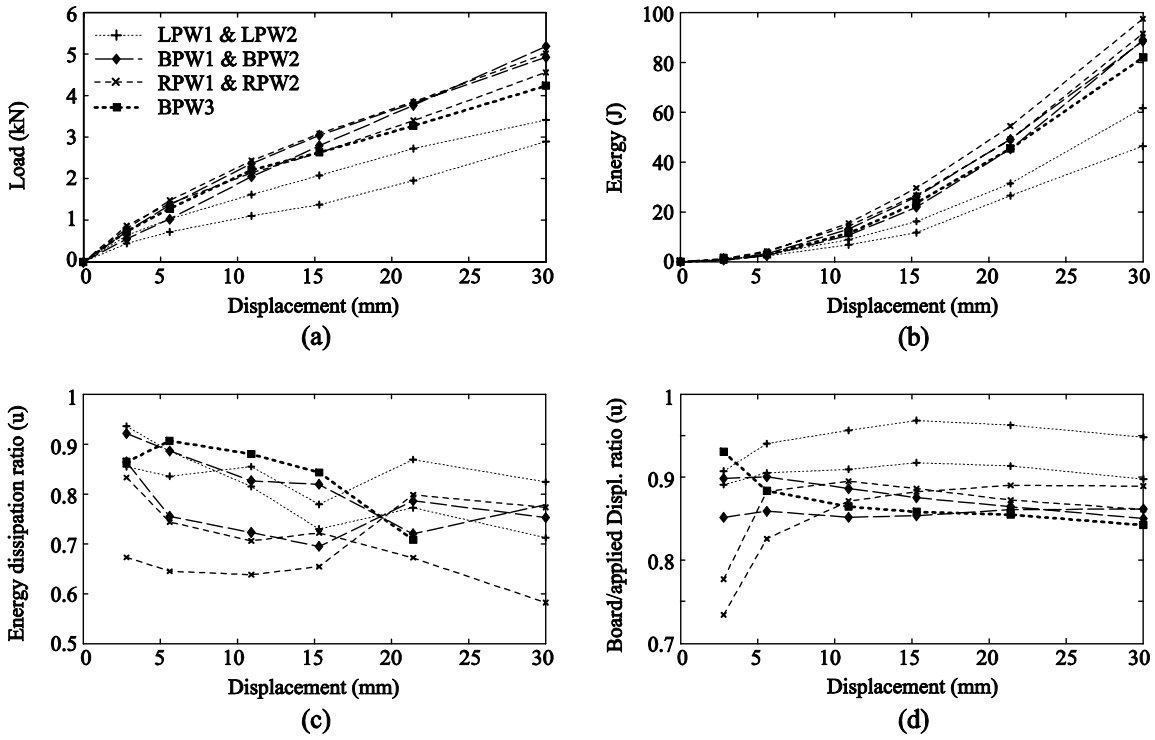


Figure 3-7: Test results of PW tests for Phase I: (a) load pushovers, (b) dissipated energy pushovers, (c) dissipated energy ratio between the second cycle and first cycle, and (d) displacement ratio between the top of the board over applied displacement by testing frame. Values per unit length of wall

The displacement and rotation of the boards relative to the framing correlates directly with the damage observed. Therefore, by reducing this displacement by conventional techniques or by energy dissipating elements, the performance of the PW can be improved. The displacement transmitted to the boards by the testing frame is analyzed in order to estimate the damage to the boards. The transmission of

displacement is taken as the ratio between the horizontal displacement of the top of the boards, point A in Figure 3-3(a), over the applied displacement by the frame. This value is denoted as board/applied displacement ratio (BDR). The results, calculated as the average between the maximum and minimum values of BDR per cycle, are shown in Figure 3-7(d). For all specimens the boards take most of the displacement applied, around 85% to 90%. The rest of the displacement is taken mainly by the deformation of the drywall screw connections. In the case of specimens of type LPW, the boards moved more than the other specimens, yet dissipated energy, as shown earlier, was lower. In the case of LPW specimens, the deformation of the framing was greater due to the thinner members, hence the relative displacement between the boards and the framing, associated with damage and energy dissipation, was lower.

Specimen BPW3 was tested to fatigue, and the variation of its strength over cycles is shown in Figure 4-9(a). It is shown that strength does not decrease significantly. For the fifth cycle at 30 mm load capacity diminished in 14% compared to the first cycle. Energy dissipation did decrease: for the fifth cycle energy was a 55% lower. These results show once again that degradation of the PW increases considerably with repetitive cycles due to the significant pinching effect.

The observed stiffnesses and load capacities of the PWs are important inputs for the design of the energy dissipating walls. Given their load capacity, the strength of the dissipating elements is selected.

# 4. ENERGY DISSIPATION PARTITION WALL (EDPW)

In the previous section, the properties of the conventional PW were obtained experimentally. This section investigates the response of an energy dissipating partition wall (EDPW), which consists of a conventional PW with a dissipating element (rail) placed at the top or bottom ends of the PW. The rail in this case is formed by metallic UFPs dampers [15]. The dissipative rail, from now on denoted as DR, is located between the top runner of the wall and the top slab (Figure 4-1). When the wall is subjected to shear deformation, the dampers inside the DR roll and yield [10]. This behaviour prevents the PW from taking more force than the yield capacity of the rail, hence preventing its damage, and increases the energy dissipation capacity of the wall.

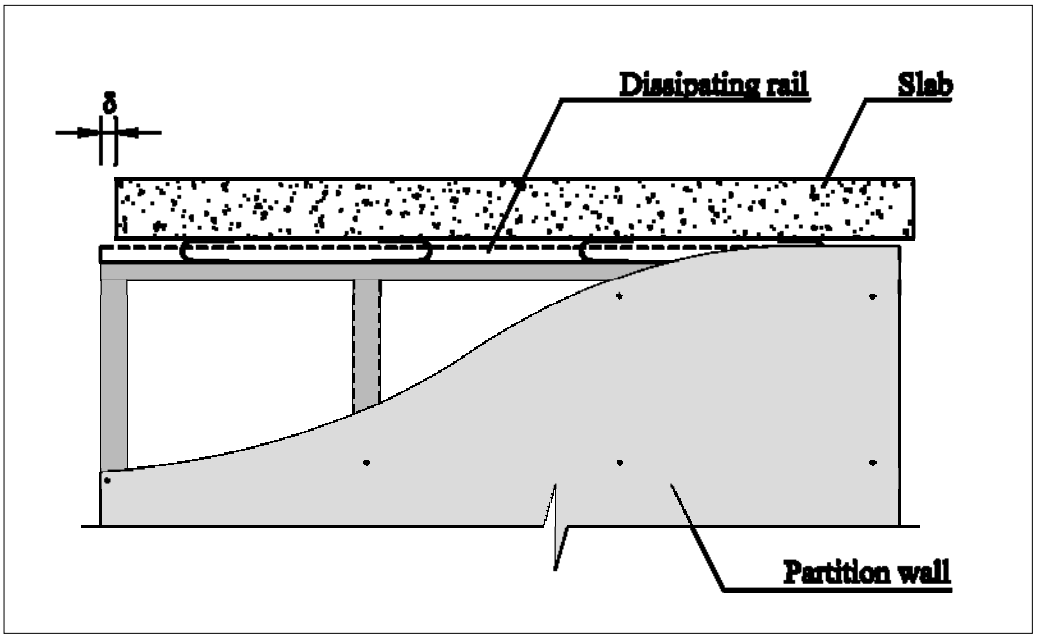


Figure 4-1: Partition wall retrofitted with dissipating rail..

### 4.1. Design of the UFP dissipators

The rail consists on a set of UFPs encased by top and bottom steel shapes. The bottom element is attached to the top runner of the PW, and the top element to the floor slab. The objective of design is that the rail undertakes most of the inter-story deformation through yielding. The calibration of the yielding capacity of the rail is done by modifying the width of the UFPs, which in turn modifies the rail capacity linearly. The DR should optimize the energy dissipation of the EDPW, but at the same time the design should minimize the deformation of the PW to concentrate as much as possible the deformation on the rail. The material used for the UFPs is annealed A36 steel. Annealing was done to eliminate any residual stresses produced during fabrication and to increase ductility.

The geometry of the UFP determines completely its hysteretic behaviour. Of all parameters used to describe the UFP (Figure 4-2(a)), the most relevant are the thickness $t$ and the internal radius $R_i$. A numerical FEM model that will be explained later was used to design and evaluate the effect of these parameters for light gauge UFPs. Results obtained by this model were used to establish the general geometries of the tested UFPs. Because it is known that the cyclic behaviour is difficult to estimate well through numerical modelling due to the highly non-linear behaviour of light-gauge UFPs, a suite of experimental results were deemed necessary.

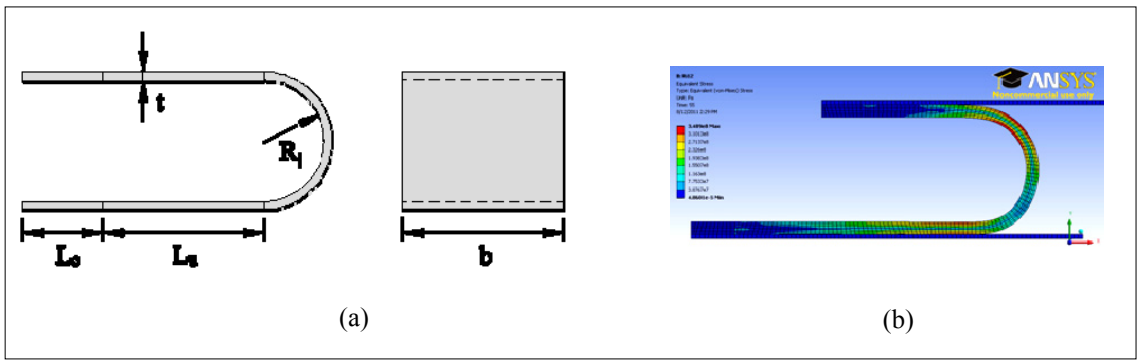


Figure 4-2: (a) Geometric parameters of the UFP, and (b) finite element model.

The UFP test program consisted of applying a sequence of shear displacements to a set of UFPs, which were selected based on the FEM simulation. The devices were made of annealed A36 steel and each test considered a set of 4 UFPs with the same geometry. The UFPs were welded to thick steel plates with a weld length of $L_c$=20 mm. These plates were bolted to a fixed test rig (Figure 4-3), and mounted on an INSTRON servo-hydraulic testing system. Displacements were applied in two stages:(i) a 0.1Hz sinusoidal displacement applied in six incremental steps: 5, 10, 20 mm and 3 cycles at 30 mm maximum amplitude; and (ii) as many cycles as needed at 30 mm displacement amplitude up to rupture of the device. Rupture was determined by visual inspection and was validated by a substantial decrease in strength.

As it is shown in Table 4-1, testing was done on 6 families of UFPs that include different plate thicknesses and internal radii. Experimental results will be later used to validate the analytical model and to define the final geometry of the proof of concept EDPW. As it is shown in Figure 4-5, all tested devices showed very stable yielding in rolling and bending. The observed cyclic transient responses of the UFPs are

characterized by an isotropic type of hardening, with a quick stabilization for repetitive cycles at same amplitude, as seen in Figure 4-5. Yielding of the specimens started at small displacements, and thus their energy dissipation capacity. Energy efficiency, taken as the ratio between the true dissipated work in a cycle and the work corresponding to the rectangle that encloses that cycle, varied for all tests from 78 to 90%.

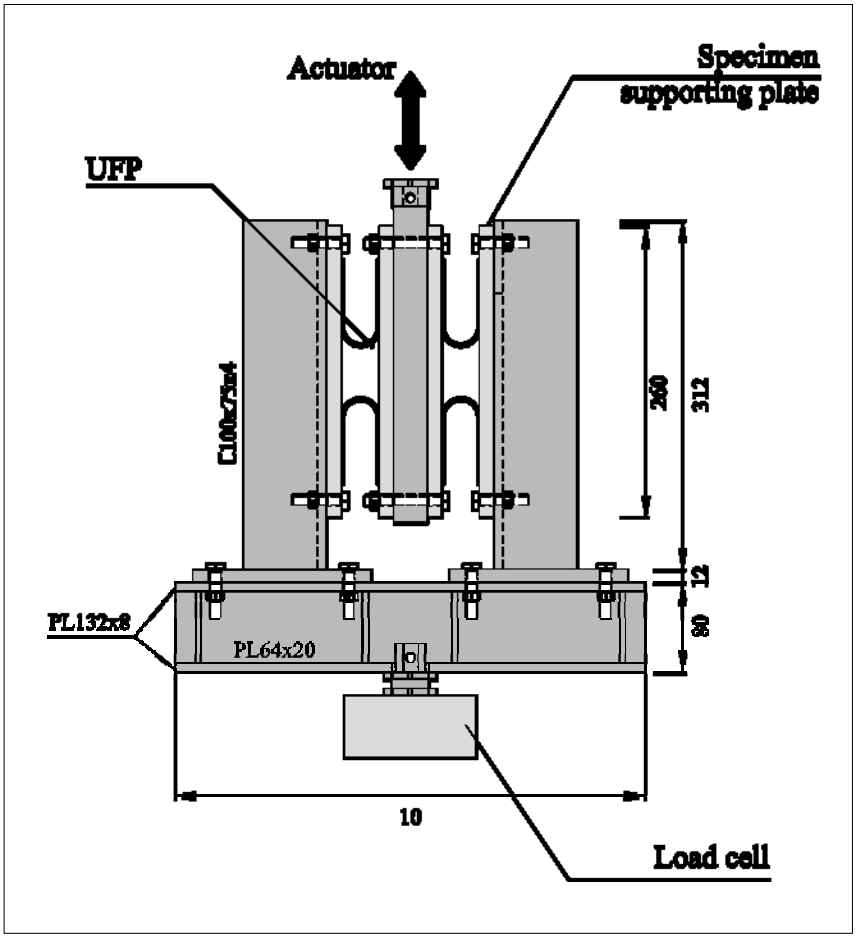


Figure 4-3: Set up of experimental testing of UFPs.

After 3 to 6 cycles the curvature at the centre of the bent section of the UFP increased (Figure 4-4(b)), deforming the UFP and creating a plate with a pointed shape, however it was the continuous bending at the meeting of the bent section and the flanges where initial cracking and later rupture of all plates occurred (Figure 4-4(b)). Although the geometry of the UFPs changed during the test, the load capacity of the plates remained very stable. Between the 3$^{rd}$ cycle at 30 mm, and the 80$^{th}$ at the same amplitude, shear load changed less than 11%. However, the dissipated energy decreased an average of 29% and 45% for the 2mm and1mm plates, respectively.

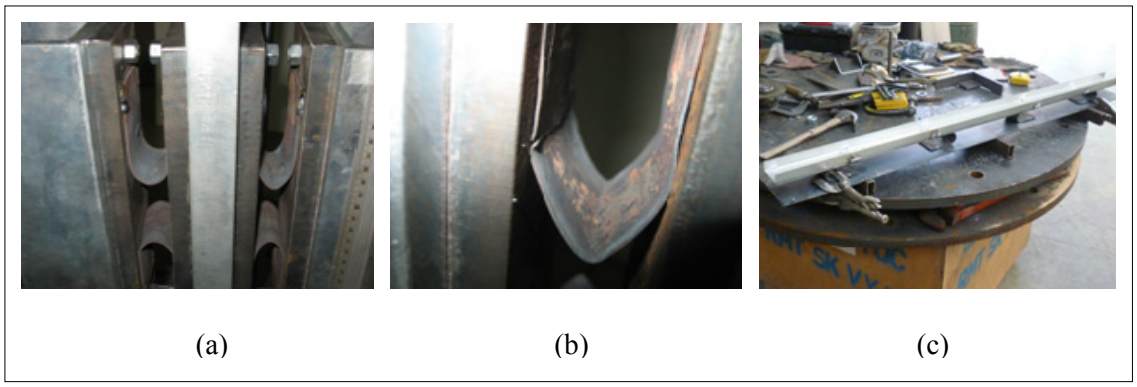

(a) (b) (c)

Figure 4-4: Photos of tests of UFP: (a) specimens mounted on testing frame, and (b) UFP after testing, showing characteristic tip and mode of failure. (c) Dissipation rail under construction.

Let us now compare the experimental and analytical responses of the UFPs. To do so, a non-linear numerical model with inelastic behaviour and large deformations of a UFP was developed in ANSYS [2] (Figure4-2). The cyclic performance of the device, while changing $t$ and $R_i$, was established for different geometries of the UFP. Although

previous FEM modelling of the UFP has been done [e.g., 14,10], this analysis is geared to low-capacity UFPs made of thin annealed A36 steel sheets.

Table 4-1: Geometric description of UFP specimens.

| Specimen | t (mm) | $R_i$(mm) | $L_U$ (mm) | $L_C$ (mm) | b (mm) |
|---|---|---|---|---|---|
| S1/12 | 1 | 12 | 40 | 20 | 50 |
| S1/15 | 1 | 15 | 40 | 20 | 50 |
| S1/18 | 1 | 18 | 40 | 20 | 50 |
| S2/12 | 2 | 12 | 40 | 20 | 50 |
| S2/15 | 2 | 15 | 40 | 20 | 50 |
| S2/18 | 2 | 18 | 40 | 20 | 50 |

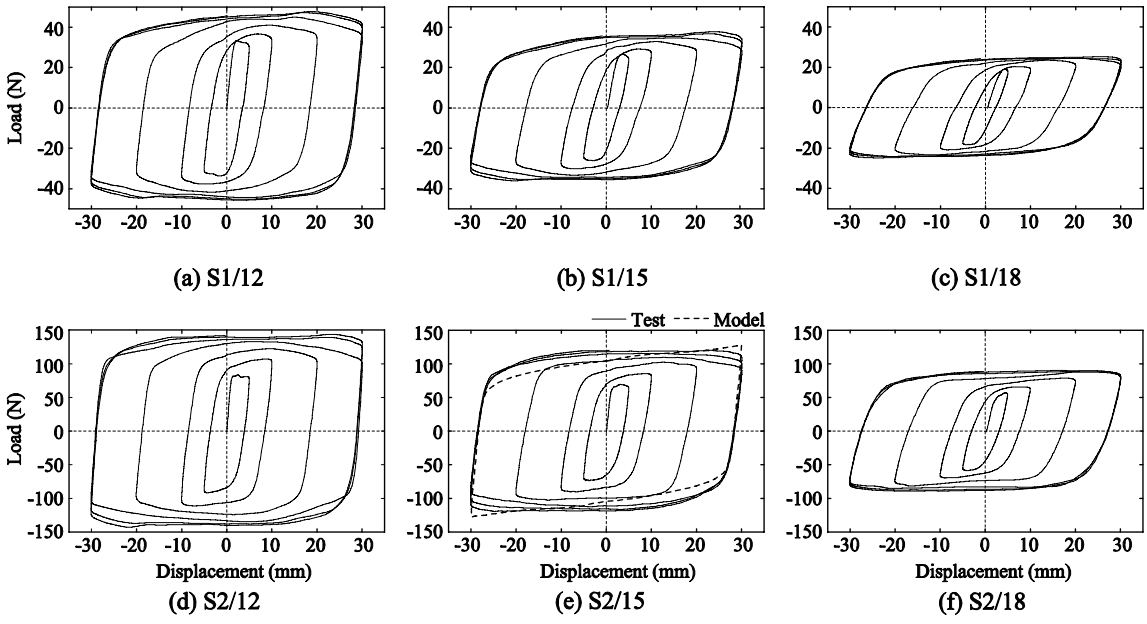


Figure 4-5: Hysteretic response of UFPs. Values per cm in width of UFP

The UFP constrained length $L_c$, free length $L_u$, and width $b$ (Figure 4-2(a)) are set in the FEM model. The constrained length is taken as 20 mm, and the width of the UFP, $b$, is assumed to be of unit width, 1cm. Different ratios of $R_i/t$ were analysed by using available commercial thicknesses of A36 sheets $t$. As the UFPs are annealed, their thicknesses reduce by the generation of a thin layer of oxide of approximately 0.1mm per side. This was included in the model by reducing the thickness of the specimen. The range of parameters $R_i$ was established based on the following qualitative observation: for low values high-strain occurs, and fatigue will cause failure of the UFP, while for high-strain values, yielding is delayed, and the energy efficiency decreases.

The A36 annealed steel was modelled with a Chaboche kinematic hardening rule [3]. Only kinematic hardening was considered because the model was intended only to predict the response for a stable cycle; the transient behaviour was not studied. When plastic flow occurs, according to this kinematic hardening relationship the yield surface $f$ relates to the Von-Misses norm $J$ of the stress and back stress tensors, $\boldsymbol{\sigma}$ and $\mathbf{X}$ respectively, and the initial size of the yield surface parameter $k$ as follows:

$$f = J(\boldsymbol{\sigma} - \mathbf{X}) - k = 0 \tag{1}$$

where the back stress tensor $\mathbf{X}$ can be written as

$$\dot{\mathbf{X}} = 2/3\, C\dot{\boldsymbol{\varepsilon}}_{\boldsymbol{p}} - \gamma \mathbf{X}\dot{p} \tag{2}$$

The back stress tensor represents the moving origin of the yield surface and it is a function of the plastic strain tensor $\dot{\boldsymbol{\varepsilon}}_{\boldsymbol{p}}$, the accumulated plastic strain $p$ and the parameters $C$ and $\gamma$. To obtain the 3 parameters needed to describe the model, a least squares curve fitting was made using the results of monotonic tests [10]. The results

obtained from these tests were a yield stress of 209MPa, an ultimate tensile stress of 369MPa, and a maximum strain of 24.8%. The elastic modulus was assumed as 2 GPa, and the values obtained for the Chaboche model were 167 MPa for $k$, 3.77GPa for $C$, and 17.2MPa for $\gamma$.

Contact at the $L_u$ length consists of gap elements with a frictional coefficient of 0.3. A 30 mm maximum displacement was applied to the top plate. Analytical results are compared next with experimental ones.

A comparison of the hysteretic response of the model and the experimental result is presented for a single representative cycle in Figure 4-5(e). It can be shown that the accuracy is reasonable, and though not shown, the rolling-bending motion can be reproduced by the model. The influence of the $R_i$ and $t$ parameters occurs as predicted by the finite element model. Load capacity, dissipated energy, and strain increased with larger $t$ and smaller $R_i$. Plate thickness was the most influential parameter for fatigue resistance; the thicker the UFP the sooner it failed. A better sense of the quality of the approximation may be obtained by the comparison of analytical and experimental results shown in Table 4-2. Analytical results of the maximum load are usually overestimated for plates with thickness of 1 mm, while the energy dissipation is underestimated. For the 2mm case results are better, and the maximum errors were 16%, 9% and 15%, for the load capacity, energy dissipation, and damping ratio, respectively. It can be shown that for light-gauge UFPs, a precise representation of the geometry and the stress-strain constitutive relationship of the material are very important. If the plate is too thin, these

variables may be slightly modified by fabrication defects, inappropriate installation, and the annealing process.

A global comparison of the analytical and experimental results is summarized in Figure 4-6.With the precautions just stated, it is apparent that the model is capable of capturing the trends of the behaviour of the UFP. The strength and energy dissipated are reasonably well represented by the model, while the equivalent damping ratio is underestimated, which is on the conservative side. The equivalent damping (Figure 4-6(c)) is also underestimated by the model, as well as for the estimations of the maximum strain, which are underestimated and overestimated by the model if $t$=1mm or$t$=2mm, respectively. Yielding of the UFP occurred mainly at the meeting of the bent section and the flanges, as it was shown by previous research [e.g., 15,1].

Table 4-2: Results from UFP model and tests

| Specimen | Results | | | | | | | |
|---|---|---|---|---|---|---|---|---|
| | Model | | | | Experimental | | | |
| | Load[(1)] (N) | Energy (J) | EE[(2)] (%) | Strain (%) | Load (N) | Energy (J) | EE (%) | Cycles (u) |
| S1/12 | 48 | 2.7 | 79 | 3.6 | 29 | 4.9 | 85 | 71 |
| S1/15 | 38 | 2.1 | 74 | 2.9 | 23 | 3.7 | 82 | 102 |
| S1/18 | 25 | 1.6 | 71 | 2.4 | 19 | 2.4 | 78 | 233 |
| S2/12 | 161 | 15.1 | 79 | 8.2 | 144 | 15.5 | 90 | 35 |
| S2/15 | 128 | 11.6 | 76 | 6.6 | 120 | 12.8 | 89 | 66 |
| S2/18 | 104 | 9.3 | 75 | 5.5 | 90 | 9.1 | 84 | 99 |

Note: Values per cm in width UFP for the third cycle at 30 mm

1. Average between maximum and minimum load of cycle
2.Energy efficiency

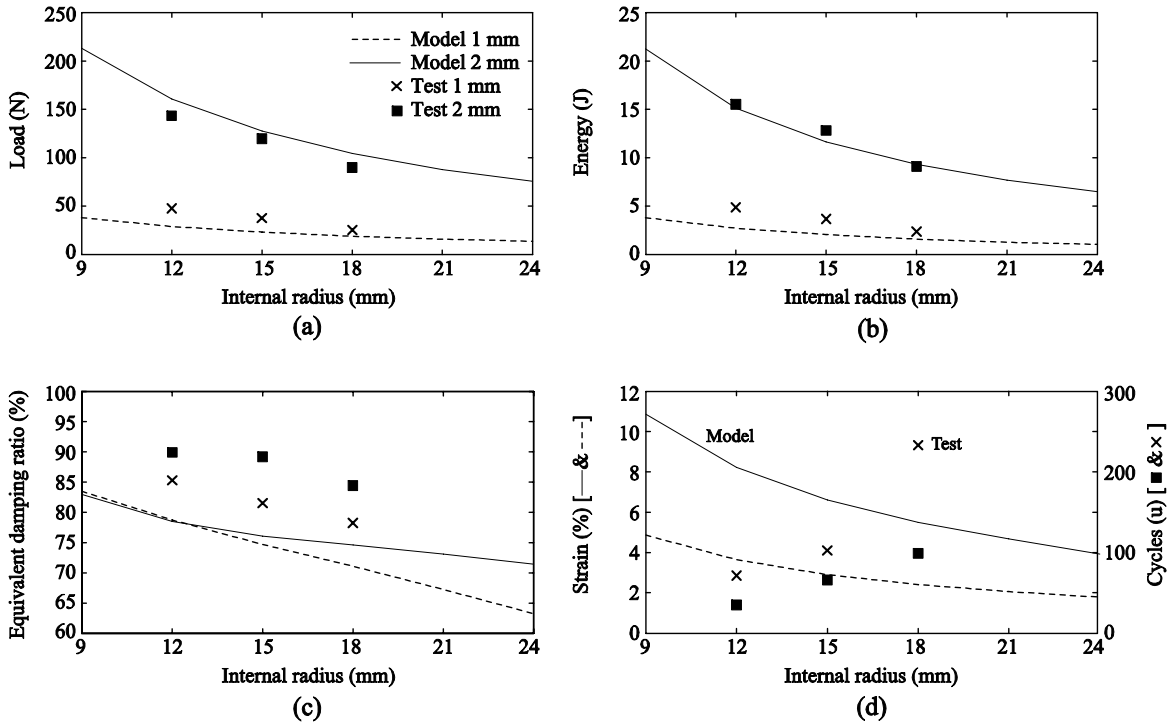


Figure 4-6: Results of the numerical model and the experimental tests of UFP: (a) load, (b) energy dissipation,(c) equivalent viscous damping, and (d) maximum strain of models and number of cycles before rupture for tests. Values per cm in width of UFP for the third cycle at 30 mm amplitude

The combinations of the design $R_i$ and $t$ parameters for the UFP must comply with two performance requirements: to limit the UFP maximum strain, and to achieve the highest possible hysteretic damping. Low strain implies a high resistance to fatigue, and based on our results should not exceed $1/4^{th}$ of the material tensile strain, which according to the monotonic test cited [10] is $\varepsilon_{max}$=6.2%. This was indeed the base for the selection of the geometries of the tested specimens shown in Table 4-1.

Based on the above experimental results and performance requirements for the UFP, the optimal design $R_i$ and $t$ parameters for the EDPW can now be selected. Assuming for the Chilean conditions that a building may undergo three important earthquakes in its lifetime, and in the case of shear wall buildings sustain a maximum of 15 cycles at a drift of 1%, the UFP should be operative up to 45 cycles before rupture. Based on these requirements the design parameters chosen were $R_i$= 15mm, and t=2 mm.

### 4.2. Behavior of the EDPW

The optimal dissipation capacity of the EDPW can be determined by adjusting the width and number of UFPs along the dissipating rail (DR).The target of the design is to maximize the energy dissipated by the PW, which will be a function of the number of UFPs, denoted hereafter as $B$, and of lateral displacement $\delta$. It also considers an upper bound limit for the lateral deformation of the PW in order to remain elastic. The problem can be written as a very simple optimization problem

$$\text{maximize } E_{EDPW}(B, \delta) \tag{3}$$

$$\text{subject to:} \quad \delta = 30 \text{ mm}$$

$$x^{PW} \leq x^{PW}_{max}$$

Where $E_{EDPW}$ is the energy dissipated by one meter of the EDPW, subjected to a deformation $\delta$ and $B$ UFP units. The constraints of the problem are self-explanatory, a target deformation of 30 mm, and a lateral deformation of the PW $\delta^{PW}$, less than the maximum deformation allowed to avoid damage. This maximum deformation is taken

from the fragility curve of gypsum sheathed PW with steel framing developed by Porter et al. [22], based on the experimental tests done by Rihal et al. [24]. According to their results, visible damage of the PW starts at a drift of about 0.3%. Because the EDPW is intended to maintain the integrity of the PW, the drift of the latter should be less than 10mm.

To evaluate in a simpler way the energy dissipated by the EDW, a numerical model is used to represent the hysteretic behaviour of the DR. The EDPW is a conventional PW in series with a DR, so the distribution of the total inter-story deformation applied $\delta$ as $\delta^{PW}$ and $\delta^{DR}$ results from the force-displacement relationship of each component. For the PW, a multi-linear model is used based on the force-displacement results obtained for the specimen BPW2 (Figure 3-7(a)), while for the DR, a simple elasto-plastic model was used considering the stiffness and yield load of $B$ UFP units. For a single unit of UFP the tangent stiffness $k$ is 65.4 N/mm, and the yielding force $f_y$, taken as the peak value of the third cycle at 30 mm amplitude, is 120 N.

Once the distribution of inter-story is obtained, the total energy dissipated can be calculated. The total energy dissipated by the PW and DR may be written as

$$E_{EDPW}(B,\delta) = \begin{cases} E_{PW}(\delta^{PW}) & \text{if } \delta^{DR} \le \delta_y^{DR} \\ 4Bf_y\left(\delta^{DR} - \delta_y^{DR}\right) + E_{PW}(\delta^{PW}) & \text{if } \delta^{DR} > \delta_y^{DR} \end{cases} \quad (4)$$

For the PW, the energy dissipated for a given deformation $E_{PW}$is taken from the energy-displacement curve obtained from specimen BPW2 (Figure 3-7(b)), while for the DR, the elasto-plastic model was used, with a yielding deformation $\delta_y^{DR}$ equivalent to $f_y/k$. Expression (4) has several assumptions that need to be considered: (a) any

behavioural interaction between the DR and PW is neglected, (b) the force-displacement and energy-displacement curves are for the virgin PW, i.e., do not consider any prior degradation, (c) the global behaviour of the DR is equivalent to the sum of the behaviour of the UFP units, (d) the DR is expected to take shear deformation only, and (e) the UFP model does not consider any isotropic hardening, and hence neglects all transient behaviour. The validity of these assumptions will be later contrasted with the observed behaviour of the EDW prototype. The optimization problem is solved for *B*, resulting in 18 cm.

As it will be shown next, three EDPWs were manufactured with two 1.2m dissipating rails each (Figure4-4(c)).Each rail contains 4 UFP elements of width 54 mm. The design of the rail used in the first specimen of the EDPWs is shown in Figure 4-7. The tests presented on the walls included improvements and iterations until reaching a final EDPW design for the proof of concept. The success is measured by: (a) the increase in the energy dissipation relative to the PW, and (b) the displacement demand reduction on the PW, which is the main factor in driving its damage.

The specifications of the three EDPW are presented in Table3-1. Gypsum sheathing and steel members are the same as those for the wall type BPW. The main modifications for the testing of these EDPW panels looked for a laterally more rigid panel, and included the insertion of the DR, strengthening of the anchoring of the wall to the bottom beam of the testing frame, and the amount of screws at the connection of runners and studs, which were increased from 1 to 2 per side, at the top and bottom.

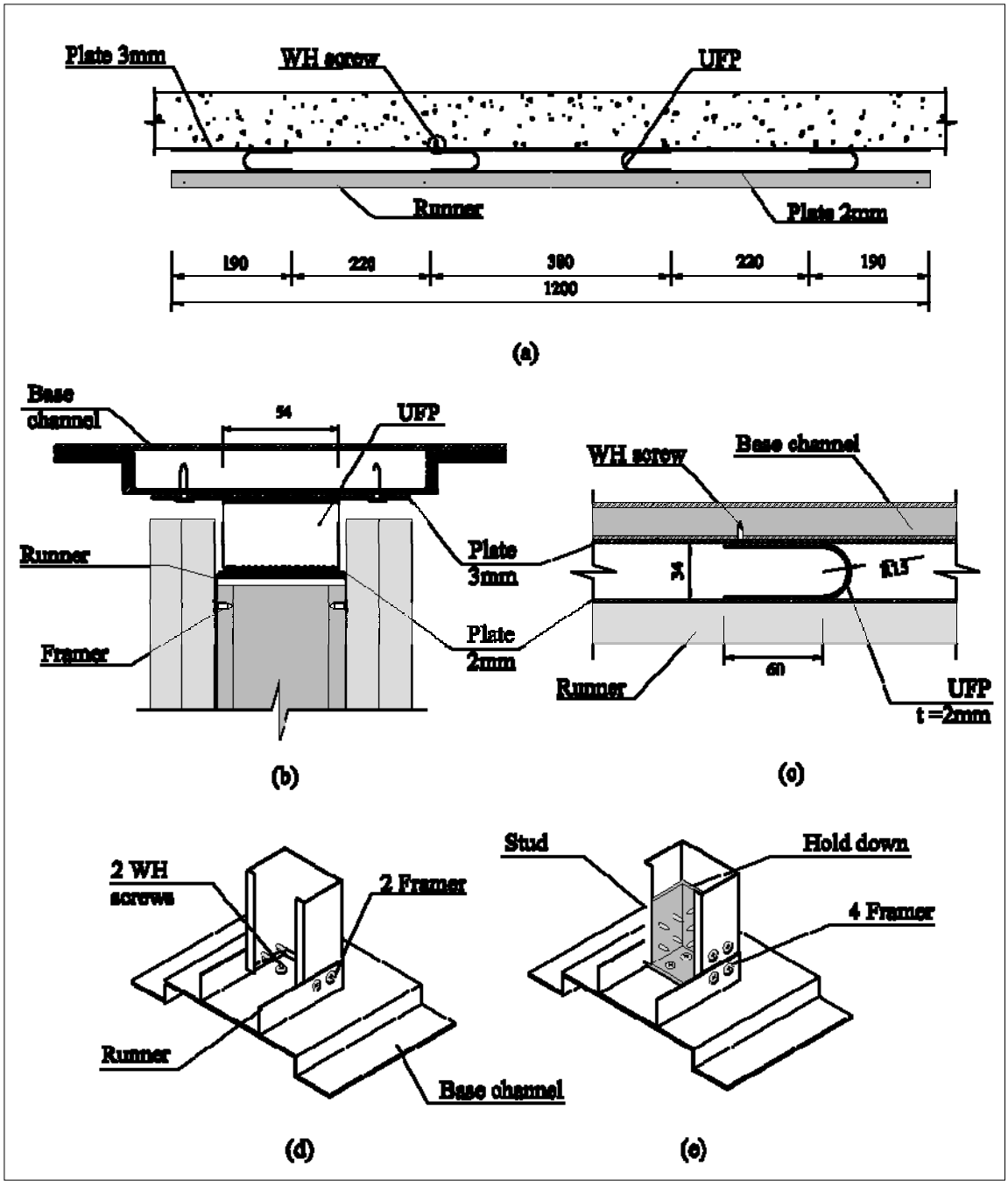


Figure 4-7: DR details: (a) general elevation when attached to concrete slab, (b) lateral section when mounted on the wall and installed in the testing frame, and (c) front detail of DR. Details of bottom anchoring of outer studs of EDPWs: (d) EDPW2, and (e) EDPW3.

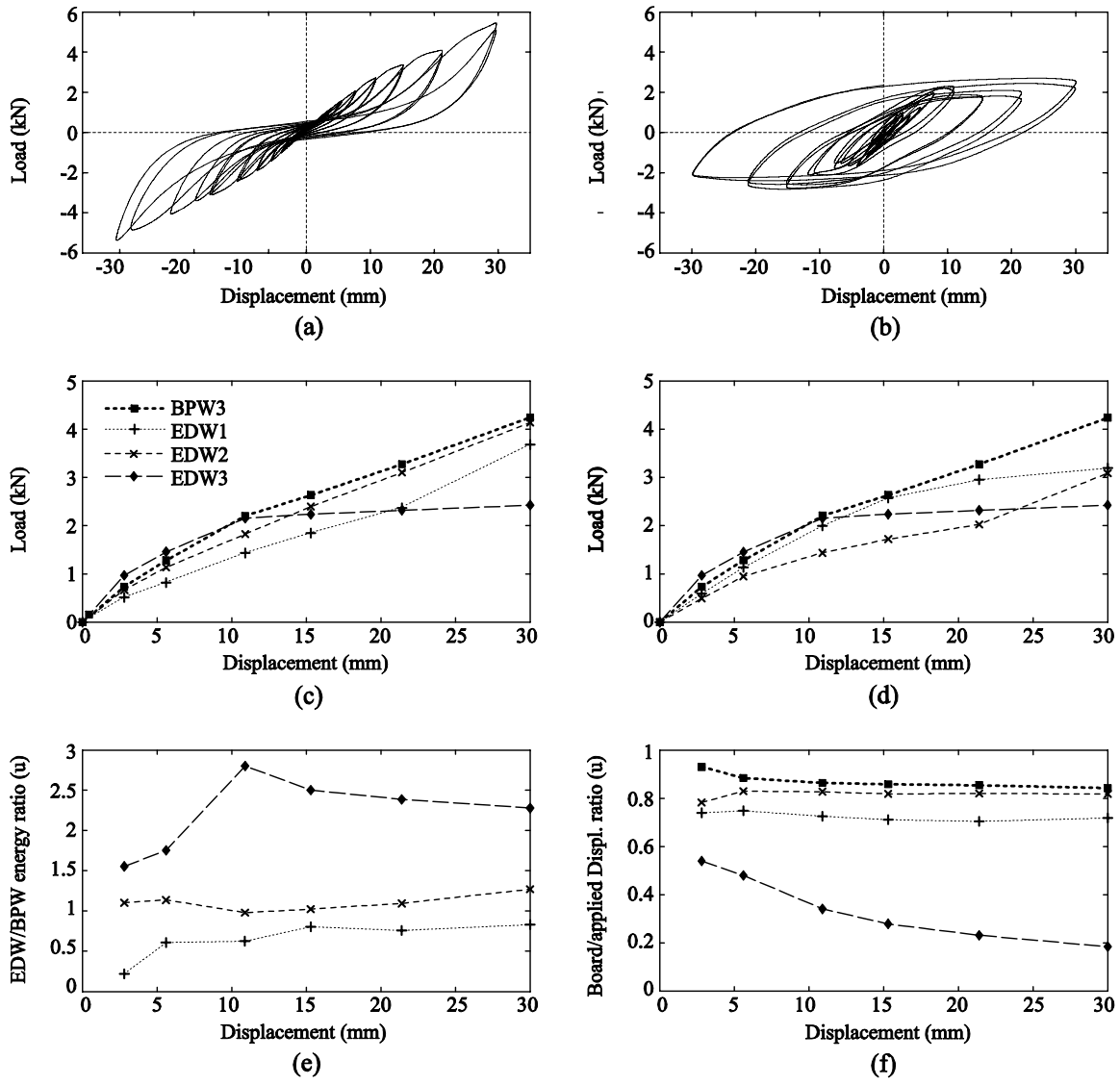


Figure 4-8: Hysteretic responses of (a) BPW and (b) EDPW3 and test results of EDPW prototypes: (c) load-displacement curves calculated as average between maximum and minimum load per cycle, (d)load-displacement curves taken as the maximum value per cycle, (e) dissipated energy of EDWs over BPW for the first cycle, and (f) displacement of the top of the board over the applied displacement of testing frame. Values per unit length of wall

The anchoring of the first prototype, specimen EDPW1, was identical to the one used for the BPW. The second specimen, EDPW2, differs from EDW1 only in the way

of anchoring the panel to the bottom channel of the testing frame, which instead of using 1 screw every 40 cm and one at 5 cm from each end of the runners, used 2 screws located precisely under each stud (Figure 4-7(d)). Specimen EDW3 is similar to EDW2, but included two differences: (i) the yield force of the dissipation rail decreased in 25% by reducing the amount of UFPs in the DR, and (ii) the studs are securely fastened to the bottom beam through hold-down brackets for the border studs and spot welding of the intermediate studs (Figure 4-7(e)).All tests were performed using the same testing frame as for the conventional PWs. Applied displacement histories were also identical to the ones used for specimen BPW3, i.e., an initial phase with incrementing amplitudes up to 30 mm, and a second phaseof80 cycles at 30 mm maximum displacement. Instrumentation and locations were also the same.

A summary of the behaviour of all three panels is presented in Figure 4-8. The behaviour of EDPW1was not as expected in design and the panel behaviour resembled that of the BPW. Rotation of the boards and uplift of runners conditioned the performance of this panel. The rolling-bending motion of the UFPs was not observed, instead bending at the centre of the bent section was produced in one direction and lifting and contraction of the flanges was produced in the other. Pinching and stiffness degradation effects are still predominant in the observed hysteretic response. The lateral load-displacement curve shown in Figure 4-8(c) was calculated by taking the average from the maximum and minimum load for each cycle. If just the maximum load is presented in the plot, as shown in Figure 4-8(d), yielding of the panel is observed. The reason for this difference is due to the high asymmetry in the load-displacement curves

that results from the asymmetric behaviour of the UFPs. In summary, the EDPW1and its DR did not work properly to limit damage within the panel. Nevertheless, it helped in identifying the most dominant factor in the performance of the EDPWs, which is the uplifting of the studs and runners.

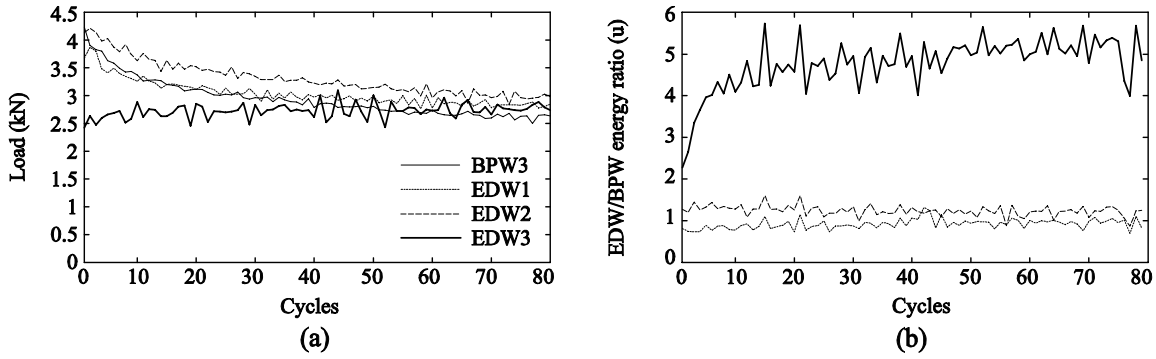


Figure 4-9: Test results of EDWs prototypes under repetitive cycles: (a) maximum load per cycle, and (b) dissipated energy of EDW prototypes over BPW.

The observed performance of specimen EDPW2 is better but not significantly than that of EDW1. In Figure 4-8(d) it is shown that the DR yielded more, though pinching and degradation are still present. The energy dissipation was increased by as much as 30% as compared to that of BPW3 (Figure 4-8(e)). In this case, the deformation of the sheathing calculated as the ratio between the horizontal displacements at the top of the board relative to the applied displacement is shown in Figure 4-8(f). By comparing to the deformation of BPW23, EDW2 reduced the deformation by 12%, which is good but not enough. Tests show that uplifting of the runners is still significant, and hence, the performance of DR is not yet effective.

Testing of specimen EDW3 shows a much better performance and complies with the proposed design for the energy dissipation wall. Yielding of the DR is significant and the pinching effects and stiffness degradation of the panel are essentially eliminated. The hysteretic response of the original specimen BPW, and the EDPW3 are compared in Figures 4-8(a) and (b). Energy dissipation is larger than that of BPW3 for all deformations and more than twice for deformations over 10 mm. This improvement increases as cycles repeat due to the degradation of the conventional PW and the very stable cyclic behaviour of the EDPW (Figure 4-9(a)). For instance, for the fifth cycle, the energy dissipation is 4 times larger and keeps increasing with the number cycles as shown in Figure 4-9(b). Moreover, the deformation of the boards is greatly reduced at all deformations, with a maximum reduction of 78% relative to that of specimen BPW3.

# 5. CONCLUSIONS

This research studied the cyclic response of conventional gypsum partition walls (PW) and walls equipped with a metallic energy dissipating element in series with the wall. Results prove that a correctly designed energy dissipating rail prevents damage on the gypsum panels as well as increases the dissipation capacity of the partition wall.

Within the experimental campaign of conventional partition walls, specimens were tested according to the FEMA 461 displacement protocol. In a second phase six were tested to large deformation and one to repetitive cycling. Some of the conclusions derived for these walls are: (i) pinching and stiffness degradation characterizes the cyclic behaviour; (ii) energy dissipation capacity is reduced between 15% to 40% from the 1$^{st}$ to the 2$^{nd}$ cycle and drifts 0.5% and 1%, respectively; (iii) stiffness and strength of the PW for drifts of 1% or less are greatly influenced by the thickness of the steel framing members, and the strength of the anchoring system between the PW and the structure; and (iv) the maximum lateral load capacity depends mainly on the capacity of the gypsum boards.

The third PW prototype with energy dissipation elements, EDPW3, proves the concept by increasing the dissipated energy of the wall more than 4 times while reducing the deformations within the panels as much as 78% for all lateral displacements. The performance improves with more cycles, and the EDPW becomes a reliable energy dissipation element for multiple seismic excitations as intended in design.

Other more specific findings derived from the analysis and testing of these elements were: (i) numerical modelling of light-gauge UFPs is complicated due to the

sensitivity to the construction defects (e.g., curvature) and uncertainties during the annealing process—for larger thicknesses analytical predictions improve greatly; (ii) the UFP hysteretic cyclic behaviour is characterized by kinematic and isotropic hardening, which needs to be included in design; (iii) the energy efficiency rate of the UFPs ranges from 0.78 to 0.9, but damping ratio decreases with a decrease in the internal radius and a smaller thickness;(iv) a relevant factor for the right performance of the EDW is the anchoring system between the PW and the structure; (v) by using the damper, displacements of the gypsum boards are reduced by as much as 78% and, hence, their integrity under cyclic loading is preserved; and (vi) for the EDPW, the energy dissipation relative to the conventional wall was 2.3 and 5 times larger for the 1$^{st}$ and 5$^{th}$ 1% drift cycles.

From a more practical standpoint, the modification proposed for the PW is highly compatible with conventional installation procedures of PWs, which makes the idea attractive to construction practice.

## REFERENCES

Aguirre, M., & Sanchez, A. R. (1992). Structural Seismic Damper. *Journal of Structural Engineering, 118*(5), 1158-1171. [1]

ANSYS Inc. (2009). ANSYS Workbench 12.0 Framework [Software]. [2]

Chaboche, J. L. (1989). Constitutive equations for cyclic plasticity and cyclic viscoplasticity. *International Journal of Plasticity, 5*(3), 247-302. [3]

Dinehart, D. W., Blasetti, A. S., &Shenton III, H. W. (2008). Experimental Cyclic Performance of Viscoelastic Gypsum Connections and Shear Walls. *Journal of Structural Engineering, 134*(1), 87-95. [4]

Earthquake Engineering Research Institute (2010). Learning from Earthquakes, The Mw 8.8 Chile Earthquake of February. Retrieved on August 15, 2011, fromhttp://www.eeri.org/site/images/eeri_newsletter/2010_pdf/Chile10_insert.pdf. [5]

Federal Emergency Management Agency (2007).*Interim Protocols for Determining Seismic Performance Characteristics of Structural and Nonstructural Components Through Laboratory Testing*. (Publication Nº FEMA461). USA. [6]

Fierro, E. A., Miranda, E., & Perry, C. L. (2011). Behavior of nonstructural components in recent earthquakes. In A. Lynn & R. Reitherman (ed.)*Proc. of the 2011 Architectural Engineering National Conference: Building Integration Solutions*(pp. 369-377)*,* Oakland, CA. [7]

Fiorino, L., Della Corte, G., & Landolfo, R. (2007). Experimental tests on typical screw connections for cold-formed steel housing. *Engineering Structures, 29*(8), 1761-1773. [8]

Fiorino, L., Della Corte, G., & Landolfo, R.(2006). Seismic response of steel frame/panel shear walls: Modelling based on screw connection tests. In F. Mazzolani & A. Wada (ed.)*Proc. of the 5th international conference on behaviour of steel structures in seismic areas- STESSA 2006* (pp. 503-510), Yokohama, Japan. [9]

Fonerón, R. A. (2007). *Muros prefabricados autocentrantes con disipadores de energía flexurales UFP.*(M. Sc. Thesis not published). Pontificia Universidad Católica de Chile, Santiago, Chile (in spanish). [10]

Freeman, S. A. (1977). Racking Tests of High-Rise Building Partitions. *Journal of the Structural Division, 103*(8), 1673-1685. [11]

Fülöp, L. A., & Dubina, D. (2004). Performance of wall-stud cold-formed shear panels under monotonic and cyclic loading: Part II: Numerical modelling and performance analysis. *Thin-Walled Structures, 42*(2), 339-349. [12]

Instituto Nacional de Normalización (1997). *Prevención de incendio en edificios - Ensayo de resistencia al fuego*. (Publication Nº NCH935). Santiago, Chile (in spanish). [13]

Kato, S., Kim, Y.-B., Nakazawa, S., & Ohya, T. (2005). Simulation of the cyclic behavior of J-shaped steel hysteresis devices and study on the efficiency for reducing earthquake responses of space structures. *Journal of Constructional Steel Research, 61(10),* 1457-1473. [14]

Kelly, J. M., Skinner, R. I. and Heine, A. J. (1972). Mechanisms of Energy Absorption in Special Devices for Use in Earthquake Resistant Structures. *Bulletin of the New Zealand Society for Earthquake Engineering, 5*(3), 63-88. [15]

Lang, A. F., & Restrepo, J. I. (2006). Seismic performance evaluation of gypsum wallboard partitions. In T. Elkhoraibi (ed.) *Proc. of the 8th U.S. National Conference on Earthquake Engineering (EERI)*, San Francisco, CA. [16]

Lee, T.-H., Kato, M., Matsumiya, T., Suita, K., & Naashima, M. (2006). Seismic performance evaluation of non-structural components: drywall partitions. *Earthquake Engineering & Structural Dynamics, 36*(3), 367-382. [17]

Matsuoka, Y., Suita, K., Yamada, S., Shimada, Y., & Akazawa, M. (2008). Non-Structural Component Performance in 4-Story Frame Tested to Collapse. *Proc. of the 14th World Conference on Earthquake Engineering*, Beijing, China. [18]

McCormick, J. (2008). Evaluation of non-structural partition walls and suspended ceiling systems through a shake table study. In D. Anderson (ed.) *Proc.of the Structures Congress 2008: Crossing the Borders, vol 314*, Vancouver, Canada. [19]

Medeot, R. (1991). Experimental testing and design of aseismic devices. *Proc. of the International Meeting on Earthquake Protection of Buildings*, Ancona, Italy. [20]

Ministerio de Vivienda y Urbanismo (1992 - updated on 2011). *Ordenanza General de Urbanismo y Construcciones*. (Publication D.S. Nº47). Santiago, Chile (in spanish). [21]

Porter, K. A., & Kiremidjian, A. S. (2001). *Assembly-based vulnerability of buildings and its uses in seismic performance evaluation and risk management decision-making*. (Report Nº 139).The John A. Blume Earthquake Engineering Center,Stanford, CA. [22]

Restrepo, J. I., & Bersofsky, A. M. (2011). Performance characteristics of light gage steel stud partition walls. *Thin-Walled Structures, 49*(2), 317-324. [23]

Rihal, S. S. (1982). Racking tests of non-structural building partitions. In S. Prakashan (ed.) *Proc. of the 7th Symposium on Earthquake Engineering, vol 1*, Meerut, India. [24]

Shinde, J. K., & Symans, M. D. (2010). Seismic Performance of Light-Framed Wood Structures with Toggle-Braced Fluid Dampers. In S. Senapathi, K. Casey & M. Hoit (ed.) *Proc. of the 2010 Structures Congress*(pp. 856-867), Orlando, FL. [25]

Symans, M. D., Cofer, W. F., & Fridley, K. J. (2002). Base Isolation and Supplemental Damping Systems for Seismic Protection of Wood Structures: Literature Review. *Earthquake Spectra, 18*(3), 549–572. [26]

Taghavi, S., & Miranda, E. (2002). Seismic Performance and Loss Assessment of Nonstructural Building Components. *Proc. of the 7th US National Conf. on Earthquake Engineering(EERI)*, Boston, MA. [27]